INVERSE PROBLEM IN OPTICAL TOMOGRAPHY USING DISCONTINUOUS GALERKIN METHOD

Y. EPSHTEYN*, T. KHAN†, AND B. RIVIÉRE ‡

Abstract. In this paper, we investigate an one dimensional inverse problem in diffusion optical tomography using the Discontinuous Galerkin (DG) method. We demonstrate that the DG method with discontinuous piecewise polynomials as a basis for the parameter space acts as an implicit regularization for the inverse problem. Our simulations suggest that DG inversion is inherently different than Continuous Galerkin (CG) inversion if the sought for parameters are discontinuous. Comparison of CG method with B-splines as a basis and the DG method with discontinuous piecewise polynomials as a basis is presented.

Key words. Inverse problems, optical tomography, discontinuous galerkin method, biomedical imaging, reconstruction algorithms

AMS subject classifications. 15A15, 15A09, 15A23

1. Introduction. Optical tomography is a way to probe highly scattering media using low-energy visible or near infra-red light and then to reconstruct images of these media. Light in the near-infrared range (wavelength from 700 to 1200 nm) penetrates tissue and interacts with it. The predominant effects are absorption and scattering [12, 15, 8]. The formation of an image for the optical properties of the tissue from a series of boundary measurements is the inverse problem. The widely accepted photon transport model is the radiative transfer equation (RTE). The RTE is an integro-differential equation for the radiance and has spatially dependent diffusion and absorption parameters as coefficients which are a priori unknown. Hence the problem is to infer from the measurements of some function of the photon density on the boundary, the coefficients of absorption and diffusion in the tissue. A low order Diffusion Approximation (DA) to the RTE has been derived and studied in the last several years. DA is an approximation to the RTE by a parabolic differential equation in the time dependent case and by an elliptic differential equation in the steady-state case [2]. The DA to the RTE has been widely used to calculate photon migration in biological tissues [16]. The existing computational methods for the inverse problem for photon migration in biological tissues are almost exclusively based on the DA [9].

It is well known that the Diffusion Optical Tomography (DOT) inverse problem is exponentially ill-posed or unstable [22, 2]. In fact, the one dimensional version of the DOT ill-posed inverse problem has been studied recently using Continuous Galerkin (CG) method [19, 4]. In order to understand the effect of Discontinuous Galerkin (DG) method on the inverse problem, we investigate the one dimensional inverse problem in DOT. The flexibility of DG methods has made these methods competitive for modeling a wide range of engineering problems. Some of the advantages of DG methods include the high order approximation, the easy implementation on nonconforming unstructured grids, the robustness and accuracy of the method for equations with discontinuous coefficients and the local mass conservation property. In this paper, we consider the non-symmetric interior penalty Galerkin method, formulated and analyzed in [24]. To our knowledge, this is the first application of DG

*Department of Mathematics, University of Pittsburgh, Pittsburgh, PA 15260.

†Corresponding Author, Department of Mathematical Sciences, Clemson University, Clemson, SC 29634-0975 (khan@clemson.edu).

‡Department of Mathematics, University of Pittsburgh, Pittsburgh, PA 15260.

to inverse problems. Theoretically, both DG and CG approximations converge to the exact solution as step size gets smaller and the degree of polynomial gets larger. However, computationally the inverse problem always depends on the choice of basis for the forward solver [5]. In fact, the DG method differs from the CG method inherently for equation with discontinuous coefficients. Therefore it is plausible that inversion of discontinuous coefficients using DG forward solver will result in a different solution than inversion using CG forward solver. Our simulations presented in this paper demonstrate that CG inversion with L_2 smoothing term such as Tikhonov regularization [13] differs from the DG solution with the same regularization. The DG method allows discontinuities in the parameters which acts as an implicit regularization apart from the L_2 Tikhonov regularization. The DG regularization is implicit because it is inherently embedded in the computational technique for the forward problem and one does not need to solve the total variation type regularization in the L_1 norm which is computationally very intensive [11].

The outline of the paper is as follows. In section 2, we discuss the forward and the inverse problem. In section 3, we describe system approximation using the DG method and the CG method. In sections 4 and 5, we describe the computational methods for the inverse problem. In section 6, we compare the solution to the inverse problem via a forward solver using DG method versus the CG method. In section 7, we discuss our results and we finish with some conclusions.

2. Forward and Inverse Problem. In optical imaging, low-energy visible light is used to illuminate the biological tissue. The illumination of the tissue can be modelled as a photon transport phenomenon. The process is described by the most widely applied equation in optical imaging, the RTE [10, 18]. Simpler deterministic models can be derived from RTE for a constant refractive index by expanding the density and the source in spherical harmonics and retaining a limited number of terms [20, 7, 3, 2].

Let $\Omega \subset \mathbb{R}^n$, $n \geq 1$ be a domain with boundary $\partial\Omega$. The DA to the RTE model can be written in the time independent case as in [2]:

$$-\nabla \cdot D\nabla u + \mu u = f \quad \text{in} \quad \Omega, \tag{2.1}$$

where $D \in L^\infty(\Omega)$ is the diffusion coefficient, $\mu \in L^\infty(\Omega)$ the absorption coefficient and $f \in L^2(\Omega)$ a source function. The resulting density u then belongs to $H^1(\Omega)$. The associated boundary condition is of Robin type:

$$u + 2D\frac{\partial u}{\partial \nu} = 0 \quad \text{on} \quad \partial\Omega. \tag{2.2}$$

The weak forward problem corresponding to equation (2.1) is: find $u \in H^1(\Omega)$ such that for all $v \in H^1(\Omega)$, the following variational equation is satisfied:

$$\int_\Omega D\nabla u \cdot \nabla v d\Omega + \int_\Omega \mu u v d\Omega + \int_{\partial\Omega} \frac{1}{2} u v ds = \int_\Omega f v d\Omega. \tag{2.3}$$

Now we can define the forward problem as: given a source f and the vector of coefficients $\mathbf{q} = (D, \mu)^T$, find the solution u on the boundary $\partial\Omega$ that satisfies (2.3) and the inverse problem as: given data z on $\partial\Omega$, find $\mathbf{q}$. We will denote $u(\mathbf{x}) = u(\mathbf{x}; \mathbf{q}, f)$ or $u(\mathbf{q}, f)$ to explicitly write the dependence of the forward solution u on the coefficients and source function. In general, measurement of $u(\mathbf{q}, f)$ may not be possible, only some observable part $\mathcal{C}u(\mathbf{q}, f)$ of the actual state may be measured. In an abstract

setting, the objective of the inverse or parameter estimation problem is to choose a parameter $\mathbf{q}^*$ that minimizes an error criterion or cost functional J over all possible $\mathbf{q}$ subject to $u(\mathbf{q}, f)$ satisfying the DA (2.1). A typical observation operator is:

$$\mathcal{C}_i^f u(\mathbf{q}, f) = -D\frac{\partial u}{\partial \nu}(\mathbf{x}_i; \mathbf{q}, f) = \frac{1}{2}u(\mathbf{x}_i; \mathbf{q}, f), \quad 1 \le i \le m \tag{2.4}$$

where m is the number of measurements, $\mathbf{x}_i$ is a point on $\partial\Omega$ and the second equality comes from the boundary condition (2.2). For example, in one dimension with $\Omega = [0, L]$, we have $m \in \{1, 2\}$ and $x_1 = 0, x_2 = L$. In this work, we employ the following typical cost functional J:

$$J(\mathbf{q}) = \frac{1}{2}\sum_{j=1}^{m_s}\sum_{i=1}^{m}\left|\mathcal{C}_i^{f_j}u(\mathbf{q}) - z_i^{f_j}\right|^2 + \lambda\|\mathbf{q} - \hat{\mathbf{q}}\|^2 \tag{2.5}$$

where $\|\cdot\|$ is the Euclidean norm, z_i^j is the measured data at the boundary point $\mathbf{x}_i$ for a given source f_j, λ is the Tikhonov regularization parameter, and $\hat{\mathbf{q}}$ is in general the vector of nominal values (corresponding to healthy tissue) for the diffusion and absorption coefficients.

3. System Approximation Using Finite Element Method. The general analytic method for solving ODEs or PDEs containing a delta distribution source is the Green's function method. However for complex geometries, the analytic solution is intractable. Therefore one requires numerical solutions. The finite element method (FEM) is more versatile than other methods including the finite difference method because of its ease in complex geometries and modelling boundary effects. The FEM is a variational method used to approximate the solution by a family of finite dimensional basis functions. Then the forward problem is reduced to one of linear algebra.

If we let $\Omega = [0, L]$ be the domain under consideration with boundary $\partial\Omega = \{0, L\}$, the weak formulation (2.3) is rewritten as: find $u \in H^1([0, L])$ such that for all $v \in H^1([0, L])$:

$$\int_0^L D(x)u'(x)v'(x)dx + \int_0^L \mu(x)u(x)v(x)dx + \frac{1}{2}u(0)v(0) + \frac{1}{2}u(L)v(L) = \int_0^L f(x)v(x)dx. \tag{3.1}$$

We first discretize the domain by considering the following subdivision

$$x_{-1} < x_0 = 0 < x_1 < ... < x_{N_p-1} < x_{N_p} = L < x_{N_p+1},$$

and stepsize,

$$h_i = x_i - x_{i-1} \text{ for } 0 \le i < N_p + 1, \quad h = \max_i h_i.$$

3.1. Continuous Galerkin Method. The classical FEM is derived by projecting the weak form (3.1) onto a finite dimensional function space V_{CG}^h, consisting of continuous and twice differentiable, piecewise cubic polynomials on the subintervals

(x_i, x_{i+1}):

$$\int_0^L D u'_{\mathrm{CG}}(x)v'(x)dx + \int_0^L \mu(x)u_{\mathrm{CG}}(x)v(x)dx + \frac{1}{2}u_{\mathrm{CG}}(0)v(0) + \frac{1}{2}u_{\mathrm{CG}}(L)v(L) = \int_0^L f(x)v(x)dx, \tag{3.2}$$

for all $v \in V^h_{\mathrm{CG}}$. We can expand u_{CG}:

$$u_{\mathrm{CG}}(x) = \sum_{i=-1}^{N_p+1} c_i^{f,\mathrm{CG}} B_i(x) \tag{3.3}$$

where $B_i(x) = B(\frac{x-x_i}{h_{i+1}})$ and B is the cubic B-spline. Thus, denoting the vector of unknowns by $\mathbf{C}_{f,\mathrm{CG}} = (c_{-1}^{f,\mathrm{CG}}, \ldots, c_{N_p+1}^{f,\mathrm{CG}})^T$ we obtain a linear system

$$A_{\mathrm{CG}}\mathbf{C}_{f,\mathrm{CG}} = \mathbf{F}_{\mathrm{CG}} \tag{3.4}$$

with $\mathbf{F}_{\mathrm{CG}} = \{\int_0^L f(x)B_i(x)dx\}_i$ and $A_{\mathrm{CG}} = D_{\mathrm{CG}} + M_{\mathrm{CG}} + P_{\mathrm{CG}}$ defined by:

$$D_{\mathrm{CG},ij} = \int_0^L D B'_i(x)B'_j(x)dx, \tag{3.5}$$

$$M_{\mathrm{CG},ij} = \int_0^L \mu B_i(x)B_j(x)dx, \tag{3.6}$$

$$P_{\mathrm{CG},ij} = \frac{1}{2}B_i(0)B_j(0) + \frac{1}{2}B_i(L)B_j(L). \tag{3.7}$$

These integrals are computed using Gaussian quadrature rules. The linear system then can be solved by standard direct or iterative methods.

3.2. Discontinuous Galerkin Method. The DG method differs from CG with respect to both the discrete space and the weak formulation. Let $V^{h,r}_{\mathrm{DG}}$ be the space of discontinuous piecewise polynomials of degree $r > 0$.

$$V^{h,r}_{\mathrm{DG}} = \mathrm{span}\{\Phi_i(x) : 1 \le i \le N_{\mathrm{dofs}}\} = \{v \in L^2(\Omega) : v|_{(x_i,x_{i+1})} = \sum_{k=1}^{r+1} \alpha_{k,i}\phi_{k,i}(x)\}. \tag{3.8}$$

Since there is no continuity constraints between the subintervals, we introduce notation for jumps $[\cdot]$ and averages $\{\cdot\}$. For this, we first denote $v(x_i^-) = \lim_{\epsilon\to 0} v(x_i - \epsilon)$ and $v(x_i^+) = \lim_{\epsilon\to 0} v(x_i + \epsilon)$, with $\epsilon > 0$. The jump and average of v at the endpoints of the subintervals of Ω are defined by:

$$[v(x_i)] = v(x_i^-) - v(x_i^+), \quad \{v(x_i)\} = \frac{1}{2}(v(x_i^-) + v(x_i^+)), \quad \forall i = 1, \ldots, N_p \tag{3.9}$$

$$[v(0)] = -v(x_0^+), \quad \{v(0)\} = v(x_0^+), \quad [v(L)] = v(x_{N_p}^-), \quad \{v(L)\} = v(x_{N_p}^-). \tag{3.10}$$

The DG solution $u_{\mathrm{DG}} \in V_{\mathrm{DG}}^{h,r}$ satisfies:

$$\forall v \in V_{\mathrm{DG}}^{h,r}, \quad \sum_{k=0}^{N_p-1} \int_{x_k}^{x_{k+1}} D(x) u'_{\mathrm{DG}}(x) v'(x) dx - \sum_{k=1}^{N_p-1} \{D(x_k) u'_{\mathrm{DG}}(x_k)\}[v(x_k)]$$
$$+ \sum_{k=1}^{N_p-1} \{D(x_k) v'(x_k)\}[u_{\mathrm{DG}}(x_k)] + \sum_{k=1}^{N_p-1} [u_{\mathrm{DG}}(x_k)][v(x_k)] + \frac{1}{2} u(0)v(0) + \frac{1}{2} u(L)v(L)$$
$$+ \sum_{k=0}^{N_p-1} \int_{x_k}^{x_{k+1}} \mu(x) u_{\mathrm{DG}}(x) v(x) dx = \int_0^L f(x) v(x) dx. \tag{3.11}$$

If we expand u_{DG}:

$$u_{\mathrm{DG}}(x) = \sum_{l=0}^{N_p-1} \sum_{k=1}^{r+1} c_{k,l}^{f,\mathrm{DG}} \phi_{k,l}(x) = \sum_{i=1}^{N_{\mathrm{dofs}}} c_i^{f,\mathrm{DG}} \Phi_i(x), \tag{3.12}$$

we obtain a linear system for the vector of unknowns $\mathbf{C}_{f,\mathrm{DG}}$:

$$A_{\mathrm{DG}} \mathbf{C}_{f,\mathrm{DG}} = \mathbf{F}_{\mathrm{DG}} \tag{3.13}$$

It is easy to check that if u is solution to (2.1), then u satisfies (3.11) (see for instance [23]). We can decompose the matrix $A_{\mathrm{DG}} = D_{\mathrm{DG}} + M_{\mathrm{DG}} + P_{\mathrm{DG}}$ where the matrices are defined by:

$$D_{\mathrm{DG},ij} = \sum_{k=0}^{N_p-1} \int_{x_k}^{x_{k+1}} D(x) \Phi'_i(x) \Phi'_j(x) dx - \sum_{k=1}^{N_p-1} \{D(x_k) \Phi'_i(x_k)\}[\Phi_j(x_k)]$$
$$+ \sum_{k=1}^{N_p-1} \{D(x_k) \Phi'_j(x_k)\}[\Phi_i(x_k)\}, \tag{3.14}$$

$$M_{\mathrm{DG},ij} = \sum_{k=0}^{N_p-1} \int_{x_k}^{x_{k+1}} \mu(x) \Phi_i(x) \Phi_j(x) dx, \tag{3.15}$$

$$P_{\mathrm{DG},ij} = \sum_{k=1}^{N_p-1} [\Phi_i(x_k)][\Phi_j(x_k)] + \frac{1}{2} \Phi_i(0) \Phi_j(0) + \frac{1}{2} \Phi_i(L) \Phi_j(L). \tag{3.16}$$

3.3. Forward Simulation. To test our forward solver for the DG method, we first computed the approximate solutions in two cases: 1) constant values of D and μ, using $f = e^{-x}$ (see Figure 3.1a for the computed solution using Dirichlet boundary condition with $N_p = 100$ and $r = 3$ and compare to analytic solution in Figure 3.1b for the forcing distribution Figure 3.1c. The absolute error plotted in Figure 3.1d), 2) constant values of D and μ using

$$f = \frac{A}{\sqrt{2\pi\epsilon^2}} e^{-\frac{|x-x_s|^2}{2\epsilon^2}} \tag{3.17}$$

with $A = 1$ and $\epsilon = 0.1$ where $x_s = 42.5$ is the source location (see Figure 3.2). Here this particular f is an approximation to the $\delta(x - x_s)$ source for which the Green's function solution is available (see Figure 3.2).

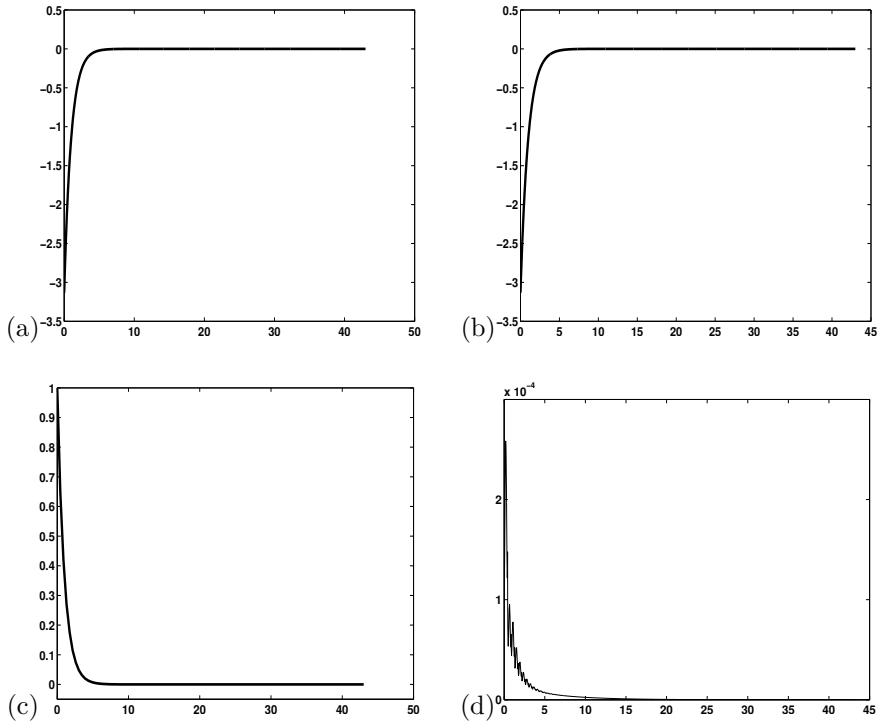

FIG. 3.1. *Constant values of D and μ, (a) DG computed solution with $N_p = 100$ and $r = 3$, (b) exact solution, (c) forcing distribution, and (d) absolute error.*

4. Computational Inverse Problem. In the previous section, we outlined the numerical method for the forward problem. In this section, we will describe the computational method for the inverse problem.

4.1. Parameter Estimation. We approximate the infinite dimensional parameters D and μ by the discrete functions D^N and μ^N for any positive integer N:

$$D^N(x) = \sum_{k=1}^{N} d_k \xi_k(x) \tag{4.1}$$

$$\mu^N(x) = \sum_{k=1}^{N} \mu_k \xi_k(x), \tag{4.2}$$

where the basis functions $\{\xi_k\}_k$ are defined on a possibly different set of grid points $\{\tilde{x}_0, \ldots, \tilde{x}_N\}$ than the subdivision $\{x_0, \ldots, x_{N_p}\}$. In general, N is different than N_p. The model parameter vector $\mathbf{q}$ is approximated by

$$\mathbf{q}^N = (d_1, \ldots, d_N, \mu_1, \ldots, \mu_N)^T \tag{4.3}$$

For the CG parameter estimation problem, the basis functions are cubic B-spines on the subintervals $(\tilde{x}_i, \tilde{x}_{i+1})$ and for the DG parameter estimation problem, the basis functions are discontinuous piecewise polynomials of degree $\tilde{r}$ on the subintervals

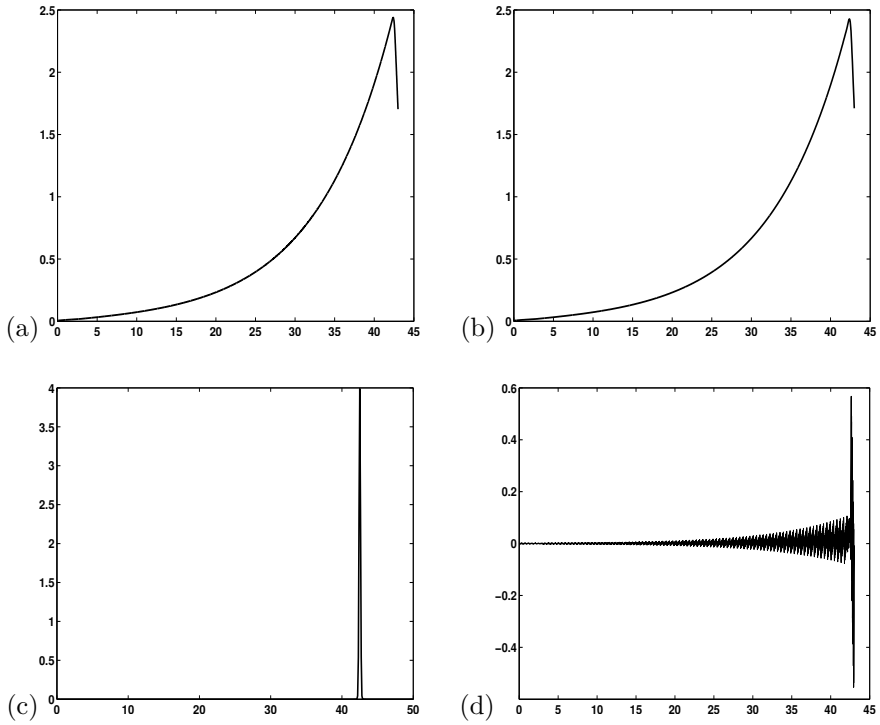

FIG. 3.2. *Constant values of D and μ, $f = \frac{A}{\sqrt{2\pi\epsilon^2}} e^{-\frac{|x-x_s|^2}{2\epsilon^2}}$ (a) exact solution for a delta distribution source, (b) DG computed solution with $N_p = 100$ and $r = 3$ for a delta distribution source, (c) approximation to the delta distribution force, and (d) computed error.*

$(\tilde{x}_i, \tilde{x}_{i+1})$:

$$D(x)|_{(\tilde{x}_i,\tilde{x}_{i+1})} = \sum_{k=1}^{\tilde{r}} d_{k,i}\phi_{k,i}(x), \quad \mu(x)|_{(\tilde{x}_i,\tilde{x}_{i+1})} = \sum_{k=1}^{\tilde{r}} \mu_{k,i}\phi_{k,i}(x). \tag{4.4}$$

4.2. Discrete Sensitivity Relations. Now we will derive the discrete sensitivity relations which will be used for the Jacobian calculation for our numerical scheme below. We differentiate (3.4) and (3.13) with respect to the components q_k^N of the discrete parameter $\mathbf{q}^N$:

$$A_{\mathrm{CG}} \frac{\partial \mathbf{C}_{f,\mathrm{CG}}}{\partial q_k^N} + \frac{\partial A_{\mathrm{CG}}}{\partial q_k^N} \mathbf{C}_{f,\mathrm{CG}} = 0 \quad 1 \le k \le 2N \tag{4.5}$$

$$A_{\mathrm{DG}} \frac{\partial \mathbf{C}_{f,\mathrm{DG}}}{\partial q_k^N} + \frac{\partial A_{\mathrm{DG}}}{\partial q_k^N} \mathbf{C}_{f,\mathrm{DG}} = 0 \quad 1 \le k \le 2N. \tag{4.6}$$

If we solve for the partial derivatives with respect to the components d_k and μ_k, we obtain in the case of CG:

$$\frac{\partial \mathbf{C}_{f,\mathrm{CG}}}{\partial d_k} = -A_{\mathrm{CG}}^{-1} D_{\mathrm{CG},k} \mathbf{C}_{f,\mathrm{CG}} \quad 1 \le k \le N \tag{4.7}$$

$$\frac{\partial \mathbf{C}_{f,\mathrm{CG}}}{\partial \mu_k} = -A_{\mathrm{CG}}^{-1} M_{\mathrm{CG},k} \mathbf{C}_{f,\mathrm{CG}} \quad 1 \le k \le N, \tag{4.8}$$

where $D_{\mathrm{CG},k}$ and $D_{\mathrm{CG},k}$ are the $(N_p+3)\times(N_p+3)$ matrices defined by:

$$(D_{\mathrm{CG},k})_{ij}=\int_0^L \xi_k(x)B_i'(x)B_j'(x)dx,\quad (M_{\mathrm{CG},k})_{ij}=\int_0^L \xi_k(x)B_i(x)B_j(x)dx. \quad (4.9)$$

Similarly for the DG case, solving for the partial derivatives with respect to d_k and μ_k yields:

$$\frac{\partial \mathbf{C}_{f,\mathrm{DG}}}{\partial d_k}=-A_{\mathrm{DG}}^{-1}D_{\mathrm{DG},k}\mathbf{C}_{f,\mathrm{DG}}\quad 1\le k\le N \quad (4.10)$$

$$\frac{\partial \mathbf{C}_{f,\mathrm{DG}}}{\partial \mu_k}=-A_{\mathrm{DG}}^{-1}M_{\mathrm{DG},k}\mathbf{C}_{f,\mathrm{DG}}\quad 1\le k\le N, \quad (4.11)$$

where $D_{\mathrm{DG},k}$ and $D_{\mathrm{DG},k}$ are the matrices defined by:

$$(D_{\mathrm{DG},k})_{ij}=\frac{\partial D_{\mathrm{DG,ij}}}{\partial d_k},\quad (M_{\mathrm{DG},k})_{ij}=\frac{\partial M_{\mathrm{DG,ij}}}{\partial \mu_k}. \quad (4.12)$$

The precise form of the entries of $D_{\mathrm{DG},k}$ and $D_{\mathrm{DG},k}$ depend on the choice of the subdivisions $\{x_0,\dots,x_{N_p}\}$ and $\{\tilde{x}_0,\dots,\tilde{x}_{N_p}\}$. In our numerical experiments, those meshes are chosen independently of each other.

5. Numerical Scheme. Now we describe our numerical scheme for the inverse problem. The inverse problem in equation (2.5) without any regularization can be casted as a finite dimensional nonlinear minimization problem mainly,

$$\min_{\mathbf{q}^N\in\mathbb{R}^{2N}} J(\mathbf{q}^N)=\frac{1}{2}\sum_{j=1}^{m_s}\sum_{i=1}^{m}\left|\mathcal{C}_i^{f_j}u^{N_p}(\mathbf{q}^N)-z_i^{f_j}\right|^2=\frac{1}{2}\|R(\mathbf{q}^N)\|^2=\frac{1}{2}\sum_{i=1}^{m_{tot}} r_i^2(\mathbf{q}^N)$$

with zero or nonzero residual, where, $R(\mathbf{q}^N)=(r_1(\mathbf{q}^N),r_2(\mathbf{q}^N),\dots,r_{m_{tot}}(\mathbf{q}^N))^T$ with $m_{tot}=m\times m_s$, $r_n(\mathbf{q}^N)=\mathcal{C}_i^{f_j}u^{N_p}(\mathbf{q}^N)-z_i^{f_j}$ with $n=i+(j-1)m$, and the norm $\|R(\mathbf{q}^N)\|$ is called the residual at $\mathbf{q}^N$. Let $\bar{H}(\mathbf{q}^N)=K^*(\mathbf{q}^N)K(\mathbf{q}^N)$, where $K(\mathbf{q}^N)$ is the Jacobian matrix of $R(\mathbf{q}^N)$,

$$K(\mathbf{q}^N)=\left(\frac{\partial r_n(\mathbf{q}^N)}{\partial q_k}\right),\ n=1,...,m_{tot},\ k=1,...,N. \quad (5.1)$$

The gradient is given by,

$$\nabla J(\mathbf{q}^N)=K^*(\mathbf{q}^N)R(\mathbf{q}^N) \quad (5.2)$$

and the Hessian is given by,

$$\nabla^2 J(\mathbf{q}^N)=\bar{H}(\mathbf{q}^N)+A(\mathbf{q}^N) \quad (5.3)$$

where $A(\mathbf{q}^N)=\sum_{i=1}^{m_{tot}} r_i\nabla^2 r_i(\mathbf{q}^N)$. Thus, if the Jacobian matrix $K(\mathbf{q}^N)$ is available, we know the first part $\bar{H}$ of the Hessian $\nabla^2 J(\mathbf{q}^N)$ without requiring any second order information.

For example, if we use an observation operator as in equation (2.4) we get:

$$\frac{\partial r_n(\mathbf{q}^N)}{\partial q_k^N}=-D\frac{\partial}{\partial q_k^N}\Big(\frac{\partial u_h}{\partial \nu}(x_i;\mathbf{q}^N,f_j)\Big)=\frac{1}{2}\frac{\partial u_h}{\partial q_k^N}(x_i;\mathbf{q}^N,f_j) \quad (5.4)$$

where u_h is either the CG or DG solution to the forward problem. We will consider both cases separately. First, if we plug the expression for u_{CG} from equation (3.3) into equation (2.4) we get:

$$\frac{\partial r_n(\mathbf{q}^N)}{\partial q_k^N} = \frac{1}{2}\sum_{l=-1}^{N_p+1} \frac{\partial c_l^{f_j,\mathrm{CG}}}{\partial q_k^N} B_l(x_i) = \bar{\mathbf{B}}^T \frac{\partial C_{f_j,\mathrm{CG}}}{\partial q_k^N} \tag{5.5}$$

where

$$\bar{\mathbf{B}} = \frac{1}{2}(B_{-1}(x_i), B_0(x_i), \ldots, B_{N_p}(x_i), B_{N_{p+1}}(x_i))^T \tag{5.6}$$

and $C_{f_j,\mathrm{CG}}$ is given by equation (3.4). Therefore using the sensitivity equations (4.7) and (4.8) for the expression $\frac{\partial C_{f_j,\mathrm{CG}}}{\partial q_k^N}$ in equation (5.5) we can compute the Jacobian matrix $K(\mathbf{q}^N)$ for the inverse calculation. One can also use the adjoint formulation to derive this Jacobian matrix which can be beneficial in two and three dimensions. However in one dimension the speed of the forward sensitivity relations is adequate to compute the Jacobian of the inverse problem. Similarly, for the DG case, we use the expression (3.12) to obtain:

$$\frac{\partial r_n(\mathbf{q}^N)}{\partial q_k^N} = \frac{1}{2}\sum_{l=0}^{N_p-1}\sum_{t=0}^{r+1} \frac{\partial c_{t,l}^{f_j,\mathrm{DG}}}{\partial q_k^N} \phi_{t,l}(x_i) = \bar{\mathbf{\Phi}}^T \frac{\partial C_{f_j,\mathrm{DG}}}{\partial q_k^N} \tag{5.7}$$

with

$$\bar{\mathbf{\Phi}} = (\phi_{1,0}(x_i), \phi_{2,0}(x_i), \ldots, \phi_{r+1,0}(x_i), \ldots, \phi_{1,N_p-1}(x_i), \ldots, \phi_{r+1,N_p-1}(x_i))^T \tag{5.8}$$

and $\frac{\partial C_{f_j,\mathrm{DG}}}{\partial q_k^N}$ is given by (4.10) and (4.11).

Given the Jacobian of the inverse problem, we can define the Iteratively Regularized Gauss-Newton (IRGN) method as follows

$$\mathbf{q}_{k+1}^N = \mathbf{q}_k^N - \gamma_k [K^*(\mathbf{q}_k^N)K(\mathbf{q}_k^N) + \lambda_k I]^{-1} \left(K^*(\mathbf{q}^N)R(\mathbf{q}_k^N) + \lambda_k(\mathbf{q}_k^N - \hat{\mathbf{q}}^N)\right),$$

where λ_k is a regularizing sequence that satisfies the conditions:

$$\lambda_k > 0, \quad 1 \le \frac{\lambda_k}{\lambda_{k+1}} \le r, \quad \lim_{k\to\infty} \lambda_k = 0.$$

The reader may consult [1], [6] and [17] for the convergence analysis of IRGN under different types of conditions on the initial guess $\mathbf{q}_0$ for the CG method. The best convergence rate was achieved when we used the iteratively regularized analog of a line search procedure suggested in [21] for the well-posed case. Namely, a backtracking strategy with $\gamma_k = \gamma_0, \gamma_0/2, \gamma_0/4$, until the following two requirements were simultaneously fulfilled:

$$J_{\lambda_k}(\mathbf{q}_{k+1}) \le J_{\lambda_k}(\mathbf{q}_k) + \delta\gamma_k < \nabla J_{\lambda_k}(\mathbf{q}_k), s_k > \tag{5.9}$$

which is the Armijo-Goldstein strategy and

$$||\nabla J_{\lambda_k}(\mathbf{q}_{k+1})|| \le \rho ||\nabla J_{\lambda_k}(\mathbf{q}_k)|| \tag{5.10}$$

which is the Wolfe type strategy. Here $\mathbf{s}_k$ is the solution to $(K^*(\mathbf{q}_k)K(\mathbf{q}_k) + \lambda_k I)\mathbf{s}_k = -(K^*(\mathbf{q}_k)R(\mathbf{q}_k) + \lambda_k \mathbf{q}_k)$. In the case of CG, we choose the parameters $\delta = 0.0001$ and $\rho = 0.99$ as in [14]. In the case of DG, no backtracking strategy is used and a constant $\lambda = \lambda_0$ was chosen.

6. Simulation Results. The optimization of the functional J was performed using the IRGN iterative method described above. After 20 iterations using the CG method with equally spaced grid points with $N_p = 40$ and $N = 20$ with $\lambda_0 = 1.0E-6$ with the choice of cubic B-splines satisfying Robin boundary condition for the solution and Neumann boundary condition for the parameter, we reconstructed the D profile for a set of 10 sources. The reconstructed profile is depicted in Figure 6.1a. The line corresponds to true D and the circles correspond to the constructed D. After 29 iterations using DG method with equally spaced grid points with $N_p = 40$ and $N = 10$ with $\lambda_0 = 1.0E-3$ with the choice of piecewise cubic polynomials $r = 3$ as a basis for the forward problem and piecewise cubic polynomials $\tilde{r} = 3$ for the the parameters, we reconstructed the D profile. The reconstructed profile is depicted in Figure 6.1b. It is evident from Figure 6.1 that the inversion using forward CG and DG method are inherently different as expected because the inversion depends on the basis functions used for the solution as well as the parameters [5]. Furthermore, the DG method is known to be more robust and accurate than CG method for equations with discontinuous coefficients. In fact, the DG method allows discontinuities in the parameters which acts as an implicit regularization apart from the L_2 Tikhonov regularization. This is evident from the comparison of CG and DG inversion shown in Figure 6.1 where the DG inversion results in a more piecewise constant solution than L_2 smoothed CG solution.

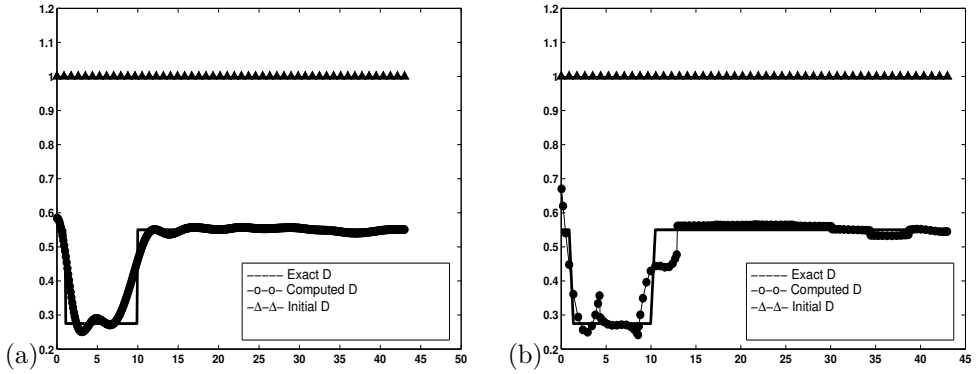

FIG. 6.1. *Comparison of CG (left) and DG (right) inversions*

In the next experiment, we vary the polynomial degrees for the DG foward and inverse problems. After 35 iterations with the choice of discontinuous linear piecewise polynomials with $\tilde{r} = 1$ and $N = 10$, we reconstructed the D profile shown in Figure 6.2a. After 30 iterations with the choice of discontinuous quadratic piecewise polynomials with $\tilde{r} = 2$ and $N = 5$, we reconstructed the D profile shown in Figure 6.2b. After 20 iterations with the choice of cubic piecewise polynomials with $\tilde{r} = 3$ and $N = 8$, we reconstructed the D profile shown in Figure 6.2c. From this experiment, we conclude that increasing the polynomial degree yields a more accurate inverse solution.

For a polynomial of degree four $\tilde{r} = 4$, we computed the inverse solution for D for three different mesh sizes $N = 5, 8$, and 10. After 18 iterations, the reconstructed profile D for $N = 5$ is shown in Figure 6.3a, after 24 iterations, the reconstructed profile D for $N = 8$ is shown in Figure 6.3b, and after 20 iterations, the reconstructed profile D for $N = 10$ is shown in Figure 6.3c. In Table 1 one can see the summary for

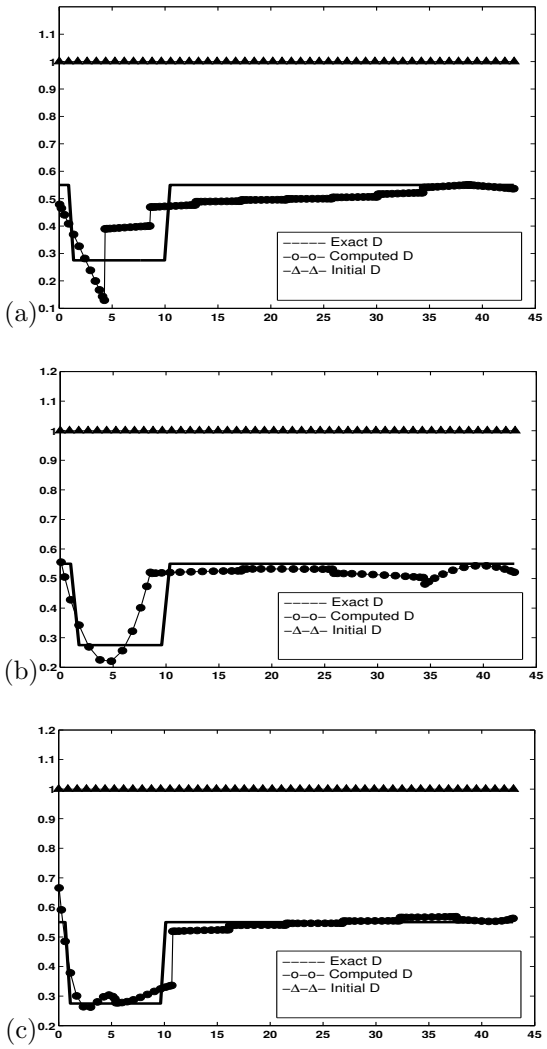

FIG. 6.2. *Inversion for three different polynomial degrees. D profile for polynomial degree (a)* $\tilde{r} = 1$*, (b)* $\tilde{r} = 2$*, and (c)* $\tilde{r} = 3$*.*

the DG inversion of measured accuracy and work done for values of λ in the range from $1.0E + 1$ to $1.0E - 4$. The best results were obtained for $\gamma = 0.25$. One can notice that the lowest residual was attained for $\lambda = 1.0E - 3$.

Table 1. Effect of Regularization Parameter for the DG Inversion

λ	L_2 Error Norm	The Residual	Number of Iterations
1.0E+1	0.1537	5.33E-1	14
1.0E+0	0.1430	8.9E-2	17
1.0E-1	0.0868	1.14E-2	22
1.0E-2	0.0716	7.83E-4	26
1.0E-3	0.0744	1.38E-5	38
1.0E-4	div	div	∞

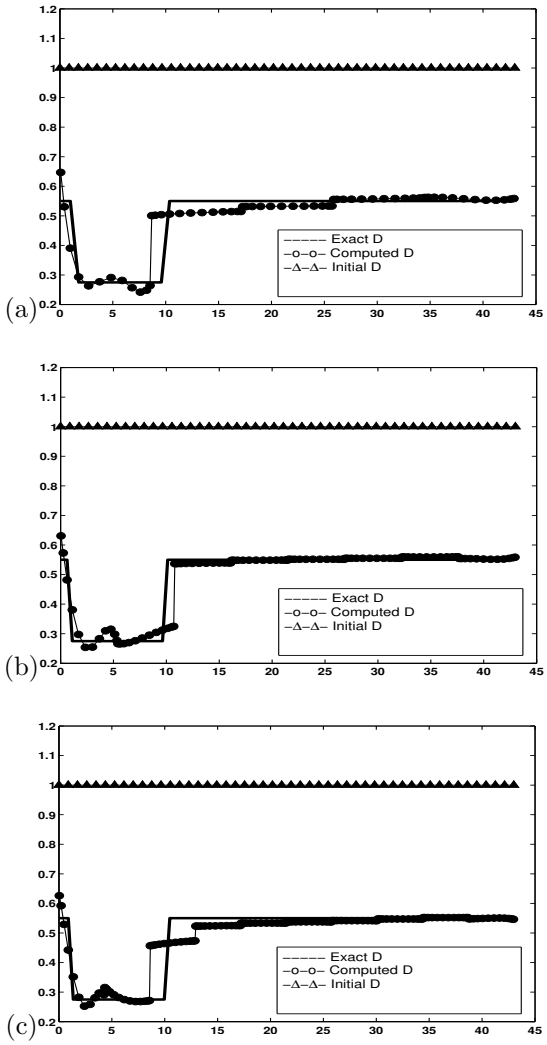

FIG. 6.3. *Inversion for three different meshes for the polynomial of degree four* $\tilde{r} = 4$. *D profile for meshes (a)* $N = 5$, *(b)* $N = 8$, *and (c)* $N = 10$.

7. Conclusion. In this paper, we investigate the one dimensional version of the inverse problem in diffusion based optical tomography. We compare the DG method to regular cubic spline CG method. We demonstrate that the DG method with discontinuous piecewise polynomials as a basis for the parameter space acts as an implicit regularization for the inverse problem. Our simulations suggest that DG inversion is inherently different than CG inversion if the sought for parameters are discontinuous. Our simulations presented in this paper demonstrate that the DG method allows discontinuities in the parameters which acts as an added regularization in addition to the L_2 Tikhonov regularization. The DG regularization is implicit because it is inherently embedded in the computational technique for the forward problem and one does not need to solve the total variation type regularization in the L_1 norm which is computationally intensive. Currently, we are performing theoretical

studies on the regularization behavior of the DG method for ill-posed problems.

REFERENCES

[1] A.B.Bakushinsky. Iterative methods for nonlinear operator equations without regularity. new approach. *Dokl. Russian Acad. Sci.*, 330:282–284, 1993.

[2] S.R. Arridge. Optical tomography in medical imaging: Topical review. *Inverse Problems*, 15:R41–R93, 1999.

[3] S.R. Arridge and J.C. Hebden. Optical imaging in medicine: 2. modelling and reconstruction. *Phys. Med. Biol.*, 42:841–853, 1997.

[4] A.B. Bakushinsky, T. Khan, and A. Smirnova. Inverse problem in optical tomog- raphy and its numerical investigation by iteratively regularized methods. *Journal of Inverse and Ill-Posed Problems*, 13(4):1–14, 2005.

[5] H.T. Banks and K. Kunisch. *Estimation Techniques for Distributed Parameter Systems*. Birkhauser, 2001.

[6] B. Blaschke, A. Neubauer, and O. Scherzer. On convergence rates for the iteratively regularized gauss-newton method. *IMA J. Num. Anal.*, 17:421–436, 1997.

[7] H. Bremmer. Random volume scattering. *Radiat. Sci. J. Res.*, 680:967–981, 1964.

[8] B. Chance and R.R. Alfano, editors. *Photon migration and imaging in random media and tissues*, volume 1888. SPIE, 1993.

[9] B. Chance and R.R. Alfano, editors. *Optical tomography, photon migration, and spectroscopy of tissue and model media: theory, human studies, and instrumentations, part 1 and 2*, volume 2389. SPIE, 1995.

[10] R. Chandrasekhar. *Radiation Transfer*. Oxford, Clarendon, 1950.

[11] T. Chen and S. Esedoglu. Aspects of total variation regularized l_1 function approximation. *UCLA CAMS Report*, 04-07:1–29, 2004.

[12] D.T. Delphy and M. Cope. Quantification in tissue near-infrared spectroscopy. *Phil. Trans. R. Soc. Lond. B*, 352:649–659, 1997.

[13] H.W. Engl, M. Hanke, and A. Neubauer. *Regularization of Inverse Problems*. Kluwer Academic Publishers, Boston, 2000.

[14] M. Hanke, J. Nagy, and C. Vogel. Quasi-newton approach to nonnegative image restorations. *Linear Algebra and Its Applications*, 316:223–236, 2000.

[15] J. Hebden, S.R. Arridge, and D.T. Delphy. Optical imaging in medicine: 1. experimental techniques. *Phys. Med. Biol.*, 42:825–840, 1997.

[16] A. Hielscher, R. Alcouffe, and R. Barbour. Comparison of finite-difference transport and diffusion calculations for photon migration in homogenous and heterogenous tissues. *Phys. Med. Biol.*, 42:1285–1302, 1998.

[17] T. Hohage. Logarithmic convergence rates of the iteratively regularized gauss-newton method for an inverse potential and inverse scattering problem. *Inverse Problems*, 13:1279–1299, 1997.

[18] A. Ishimaru. *Single Scattering and Transport Theory (Wave Propogation and Scattering in Random Media I.* Academic, New York, 1978.

[19] T. Khan and A. Smirnova. 1d inverse problem in diffusion based optical tomography using iteratively regularized gauss-newton algorithm. *Applied Mathematics and Computation*, 161:149–170, 2005.

[20] H.W. Lewis. Multiple scattering in an infinite medium. *Phys. Rev.*, 78:526–529, 1950.

[21] S.G. Nash and A. Sofer. *Linear and Nonlinear Programming*. McGraw-Hill, New York, 1996.

[22] F. Natterer and F. Wübbeling. *Mathematical Methods in Image Reconstruction*. SIAM Monographs on Mathematical Modeling and Computation, 2001.

[23] B. Rivière, M. F. Wheeler, and V. Girault. A priori error estimates for finite element methods based on discontinuous approximation spaces for elliptic problems. *SIAM J. Numer. Anal.*, 39:902–931, 2001.

[24] B. Riviére, M.F. Wheeler, and V. Girault. Improved energy estimates for interior penalty, constrained and discontinuous galerkin methods for elliptic problems: Part 1. *Computational Geosciences*, 8:337–360, 1999.